Numerical simulation of hypersonic equilibrium-air reactive flow

Jean-Antoine Desideri, Elie Hettena

INRIA

UNITÉ DE RECHERCHE
INRIA-SOPHIA ANTIPOLIS

Institut National
de Recherche
en Informatique
et en Automatique

Domaine de Voluceau
Rocquencourt
B.P.105
78153 Le Chesnay Cedex
France
Tél.(1)39 63 55 11

Rapports de Recherche

N° 716

NUMERICAL SIMULATION OF HYPERSONIC EQUILIBRIUM-AIR REACTIVE FLOW

Jean-Antoine DESIDERI
Elie HETTENA

AOUT 1987

NUMERICAL SIMULATION OF HYPERSONIC EQUILIBRIUM-AIR REACTIVE FLOW

Simulation numérique d'écoulements hypersoniques réactifs à l'équilibre chimique

Jean-Antoine DESIDERI and Elie HETTENA

INRIA Sophia-Antipolis
Avenue Emile Hughes
(Anc. Route de Lucioles)
Sophia-Antipolis
06565 VALBONNE Cedex

Abstract

This document reports recent experiments in the development of numerical methods for the simulation of reactive hypersonic flow such as the flow around a space shuttle during the atmospheric reentry (M_∞ between 15 and 25, high angle of attack). The flow slover realizes a "Finite Volume" discretization of the governing equations (Euler or Navier-Stokes). In the present approach, chemistry is accounted for via an algebraic equilibrium model. This work is mainly concerned with steady-state solutions over two-dimensional blunt-body geometries, and more specifically that of a half-cylinder.

The current research emphasizes the numerical aspects related to the capture of the strong shock (robust solver and mesh adaption) and the simulation of the dissociation phenomenon in the shock layer.

Résumé

Ce rapport présente les résultats d'une série d'expériences numériques qui s'insérent dans le cadre plus large du développement de méthodes pour la simulation des écoulements hypersoniques réactifs, tels que ceux qui se produisent autour d'une navette spatiale lors de sa réentrée dans l'atmosphère (M_∞ de 15 à 25, forte incidence). La méthode de résolution est basée sur une discrétisation par "Volumes Finis" des équations de l'aérodynamique (Euler ou Navier-Stokes). Ici, la chimie est introduite par un modèle d'équilibre. Dans cette étude, on s'interesse aux solutions stationnaires autour de corps arrondis bidimensionnels, et plus spécifiquement autour d'un demi cylindre.

Ce document est principalement orienté sur les aspects numériques liés à la capture d'un choc fort (solveur robuste et adaptation de maillage) et à la simulation de phénomènes de dissociation chimique dans la couche de choc.

Contents

I. FLOW EQUATIONS AND SOLVER

1. Discretization

For the purpose of a finite-volume formulation of the problem, the computational domain is discretized by quadrangles allowing a (j,k) indexing (see Figure 1). The degrees of freedom are placed at the vertices and in particular along the body surface. The medians of the segments are drawn to define the finite-volume cells $\{C_{j,k}\}$ about the nodes.

2. Euler calculations

Conservative solutions to the Euler equations expressed in integral form,

$$\frac{d}{dt}\int_{\mathcal{A}} w d\mathcal{A} + \int_{\partial\mathcal{A}} (f(w)n_x + g(w)n_y)ds = 0 \tag{1}$$

are captured by a finite-volume formulation combined with the Euler explicit time-integration scheme. The definitions of the conservative variables w and the flux vectors are classical,

$$w = \begin{pmatrix} \rho \\ \rho u \\ \rho v \\ E \end{pmatrix} \quad ; \quad f(w) = \begin{pmatrix} \rho u \\ \rho u^2 + p \\ \rho uv \\ (E+p)u \end{pmatrix} \quad ; \quad g(w) = \begin{pmatrix} \rho v \\ \rho uv \\ \rho v^2 + p \\ (E+p)v \end{pmatrix} \tag{2}$$

$\mathcal{A}$ is an arbitrary control area, and $\vec{n} = (n_x, n_y)$ is the corresponding outward normal vector. Hence, letting $\mathcal{A} = C_{j,k}$, (1) is discretized as follows:

$$A_{j,k} w_{j,k}^{n+1} = A_{j,k} w_{j,k}^{n} - \Delta t \left(\sum_{i=1}^{4} \Phi_{j,k}^{n}(i) \right) \tag{3}$$

where $A_{j,k}$ denotes the area of the cell $C_{j,k}$ and $\Phi_{j,k}^{n}(i)$ denotes the net flux through the interface (i). This terms incorporates a version of van Leer's flux-vector splitting [1] developed by Fezoui et al. [2] in a very general context. To define it precisely, we

consider the first interface, the arc AIB of Figure 1, the other terms being similar. Let

$$\eta_x = \int_{AIB} n_x ds \;\; ; \;\; \eta_y = \int_{AIB} n_y ds \tag{4}$$

and

$$h(w) = \eta_x f(w) + \eta_y g(w) \tag{5}$$

Then one uses a property of invariance of the flux vectors of the Euler equations by rotation,

$$h(w) = \|\eta\| R^{-1} f(Rw) \tag{6}$$

to apply the particular one-dimensional flux-vector splitting of [1], yielding

$$\Phi^n_{j,k}(1) = h^+(w^n_{j,k}) + h^-(w^n_{j+1,k}) \tag{7}$$

This form combines the advantage of continuously differentiable flux vectors (in particular, the split flux vectors are not singular at sonic points) with greater computational simplicity over other more complex Riemann solvers.

At inflow, freestream conditions are enforced. At outflow, no boundary condition is appplied; the flux-splitting automatically extracts the pertinent information from the data specified initially. Along the body, the slip condition

$$\vec{V} . \vec{n} = 0 \tag{8}$$

allows us to reduce an integral to a pressure term.

The method is only first-order accurate but it is robust, capable in particular to sharply capture strong shocks. In another context [3] it revealed particularly efficient when drastic changes in geometry occurred due to mesh adaption. Also in this way, one can avoid the dilemma of either constructing a complex and costly artificial viscosity term or obtaining very smeared and oscillatory shocks. Lastly, this explicit method is stable under a CFL-like condition comparable to that derived by Lerat [4].

3. Navier-Stokes calculations

The above finite-volume Euler code has been extended to solve the Navier-Stokes equations.

In the governing equations, the viscous terms appear at the right-hand side of (1) by the additional term:

$$T = \int_{\mathcal{A}} (R_x + S_y) d\mathcal{A} = \int_{\partial \mathcal{A}} (R n_x + S n_y) ds \tag{9}$$

where the vectors R and S are given by:

$$R = \begin{pmatrix} 0 \\ \tau_{xx} \\ \tau_{xy} \\ u\tau_{xx} + v\tau_{xy} + q_x \end{pmatrix} \; ; \; S = \begin{pmatrix} 0 \\ \tau_{xy} \\ \tau_{yy} \\ u\tau_{xy} + v\tau_{yy} + q_y \end{pmatrix} \tag{10}$$

in which the rate of strain tensor is given by:

$$\begin{cases} \tau_{xx} = \dfrac{2\mu}{3}\left(2\dfrac{\partial u}{\partial x} - \dfrac{\partial v}{\partial y}\right) \\ \tau_{xy} = \mu\left(\dfrac{\partial u}{\partial y} + \dfrac{\partial v}{\partial x}\right) \\ \tau_{yy} = \dfrac{2\mu}{3}\left(2\dfrac{\partial v}{\partial y} - \dfrac{\partial u}{\partial x}\right) \end{cases} \tag{11}$$

and the heat-conduction flux by Fourier's law:

$$\overrightarrow{q} = -k\overrightarrow{\nabla T} \tag{12}$$

Hence we again need to evaluate an integral along each cell boundary. For this we proceed as follows: for each quadrangle and for each necessary variable (u, v, etc) a least-square fit of the data at the 4 nodes by the best 1st-degree polynomial is evaluated; by differenciating this polynomial, average values of gradients are obtained; these are used to define $\overline{R}_{j,k}$ and $\overline{S}_{j,k}$ that are average values over a quadrangle; then the following (partial) contribution to the integral T over the cell $C_{j,k}$ is computed:

$$\delta T_{j,k} = \overline{R}_{j,k} \int_{IBJ} n_x ds + \overline{S}_{j,k} \int_{IBJ} n_y ds \tag{13}$$

This term is multiplied by Δt and added to the right-hand side of (2). Proceeding in this way, the calculation of the NS-terms is performed with a loop over the quadrangles. After completion of the loop, 4 corrections similar to that of (13) have affected a given (interior) cell. Note that the corrections brought to the difference equations at opposite nodes of the same quadrangle are opposite. At nodes of the interior, this approximation is a form of central differencing. At the outflow boundary, it becomes (1st-order) backward differencing.

In addition, the boundary procedure has been modified to account for the no-slip condition ($u = v = 0$) and the condition of adiabatic wall ($\partial T/\partial n = 0$) is enforced with a finite-difference.

II. EQUILIBRIUM MODEL

Up to date, we have used a numerical model constructed at AMD-BA by B. Stoufflet and M. O. Le Ber [5] [11]. In this model, the gas is made of 5 species (N_2, O_2, N, O and NO) and 3 major equilibrium equations are extracted from the more complete dissociation model by Rakich [6]:

$$\begin{cases} O_2 + X \rightleftharpoons 2O + X \\ N_2 + X \rightleftharpoons 2N + X \\ N_2 + O_2 \rightleftharpoons 2NO \end{cases} \tag{14}$$

where X represents an arbitrary collision factor (any other species). The law of mass action is thus expressed as follows:

$$\begin{cases} \dfrac{Y_2^2}{Y_5} = \dfrac{m_2^2}{m_5}\dfrac{K_2(T)}{\rho} \\ \dfrac{Y_1^2}{Y_4} = \dfrac{m_1^2}{m_4}\dfrac{K_1(T)}{\rho} \\ \dfrac{Y_3^2}{Y_4 Y_5} = \dfrac{m_3^2}{m_4 m_5} K_6(T) \end{cases} \tag{15}$$

in which the Y_i's for $i = 1, 2, .., 5$ are the mass fractions of N, O, NO, N_2 and O_2 respectively, and the m_i's their respective molar masses. In this way, the values 1, 2 and 3 of the subscript are associated with the "chemical products" of the species that are not present below a certain temperature T_0 ($T_0 = 298\ K$), and in particular in the undisturbed flow. For the equilibrium constants we have employed the same expressions as in [6].*

* In Table 1 of [6], we understand

$$K_1(T) = \left(\rho \frac{q_1^2}{q_4}\right)_e$$

where ρ is the local value of density, and the same for $K_2(T)$ and $K_3(T)$. Also the factor $\exp(-21500T^{-1})$ should not appear in $K_6(T)$.

The mass fractions satisfy two algebraic equations. First, evidentally:

$$\sum_{i=1}^{5} Y_i = 1 \tag{16}$$

Second, if the diffusion of the species is neglected, the local proportion of oxygen atoms relative to nitogen atoms is uniform and this gives. written as follows:

$$\frac{\frac{Y_1}{m_1} + \frac{Y_3}{m_3} + 2\frac{Y_4}{m_4}}{21} = \frac{\frac{Y_2}{m_2} + \frac{Y_3}{m_3} + 2\frac{Y_5}{m_5}}{79} \tag{17}$$

Hence only 3 mass fractions are independent.

Note that once a temperature estimate is known, (2-4) can be solved for the mass fractions.

Each individual species is treated as a perfect gas with constant specific heats ($C_p = \frac{7}{2}R$ for N_2, O_2 and NO and $\frac{5}{2}R$ for N and O). The state equation has the form:

$$p = \rho \mathcal{R} T \sum_{i=1}^{5} \frac{Y_i}{m_i} \tag{18}$$

Finally, one needs to relate energy, temperature and mass fractions. For this, the total enthalpy per unit mass is first expressed:

$$h = \frac{V^2}{2} + \sum_{i=1}^{3} Y_i h_i^0 + \sum_{i=1}^{5} Y_i C_{p_i}(T - T_0) \tag{19}$$

where $V^2 = u^2 + v^2$ and h_i^0 is the formation enthalpy of the species i at the reference temperature T_0 ($T_0 = 298K$). The total energy per unit volume is then

$$E = \rho h - p \tag{20}$$

Note that this equation can be solved for the temperature once the mass fractions are estimated, all other properties being given by the solution of the flow equations.

III. ALGORITHM

First the flow equations (Euler or Navier-Stokes) are solved forward in time over one timestep, using a local value of the following parameter (obtained at every cell center at the previous timestep):

$$\gamma = \frac{h}{e} \tag{21}$$

where e is the internal energy per unit mass:

$$e = \frac{E}{\rho} - \frac{V^2}{2}$$

Then the temperature and the mass fractions are calculated by solving (1-4) iteratively.

At convergence the value of γ is updated in preparation of the next timestep.

Note that this parameter does not appear explicitly in the partial differential equations; therefore it only affects the artificial viscosity inherent to the chosen flux splitting.

The process is continued until the steady state is achieved.

IV. MESH ADAPTION

In this problem, the shock and, for Navier-Stokes solutions, the boundary-layer require greater resolution. To capture these structures economically, a one-dimensional mesh adaption very similar to the "static rezone" of [7] was employed.

Every say 500 timesteps, a new mesh is constructed, the solution interpolated onto it and the time integration proceeds.

Technically, an sensor of the local Mach gradient, or criterion function is computed along a given ray (θ = constant, or j = constant). The following form revealed adequate:

$$w = a + bd_r + cd_{rr} \tag{22}$$

where

$$d_r = \frac{\left|\frac{\partial M}{\partial r}\right|}{\max\left|\frac{\partial M}{\partial r}\right|}, \quad d_{rr} = \frac{\left|\frac{\partial^2 M}{\partial r^2}\right|}{\max\left|\frac{\partial^2 M}{\partial r^2}\right|} \tag{23}$$

and a, b and c are constants close to 1. Then the points are redistributed along the ray so that

$$\overline{w} = \int_{r_w}^{r} w(r)dr \tag{24}$$

be a linear function of the index k, if the cell centers are subscripted (j,k), i.e., linear in the *computational* radial coordinate, and precisely not directly in r.

In fact, although the adaption is made one-dimensionally, a 2D smoothing of the criterion w is performed to produce more regular meshes. This is done by solving two scalar tridiagonal systems,

$$(I - \epsilon\delta_{jj})\,(I - \epsilon\delta_{kk})\,w' = w \tag{25}$$

with $\epsilon = 5$ and using the function $w'(r)$ instead of $w(r)$ in (13).

This technique is very adequate to cluster cells in the strong shock. However for Navier-Stokes solutions, it cannot refine the mesh near the wall as it should. Nevertheless, to achieve this, the criterion function $w(r)$ is currently directly modified. In particular, a quantity proportional to $\|\text{rot } V\| = \|\text{curl } V\|$ can also be included in (22) to detect sudden flow variations in the shock and the boundary layer.

V. RESULTS

The first experiments are validation tests of the method for the computation of nonreactive flowfields.

First, two calculations were made of the same inviscid flow at $M_\infty = 25$: one with a 31×61 uniform mesh and the other with a 61×121 mesh. The corresponding Mach and temperature contours are shown on Figure 2. No significant differences between the two are visible, thus demonstrating the convergence of the approximation as the mesh refines, and also that a sufficient accuracy is achieved with a calculation over a 31×61 uniform mesh. In both cases the shock is captured very sharply and the solution away from the shock is free of oscillations. This merit is partly owed to the upwind differencing. We should note however that the smoothness is also due to the use of a first-order method. These tests also demonstrate the great robustness of the upwind approximation. A computed maximum temperature of about 29000 K is observed at the stagnation point.

The effect of the freestream Mach number on the flowfield is then evaluated on Figure 3. In the hypersonic regime, the stand-off distance is essentially independent of M_∞. Indeed we observe that it only increases very slightly when M_∞ diminishes. The Mach contours are almost invariant in most of the shock layer. However, the temperatures are importantly reduced.

To test the Navier-Stokes solver, the cases corresponding to the same freestream Mach number were computed at a Reynolds number of 1000. As shown on Figure 4, the shock remains relatively sharp, but a boundary layer forms, captured within 2 to 3 cells. As a result, the stand-off distance increases. The peak of temperature does not change significantly, but the effect of diffusion is very apparent on the temperature contours.

On Figure 5, are shown the results of a calculation made with a 41×21 adapted mesh. The shock is again captured very sharply as demonstrated both by the Mach/temperature contours and the Mach/temperature plots. This accurate computation of a hypersonic flowfield ($M_\infty = 15$) is performed with only about 800 points.

We now turn to the validation of the chemical dissociation model alone. For this, the equilibrium composition of air was calculated as a function of temperature for a total pressure equal to 10^{-2} atm, the density being given by the state equation.

The results are plotted in terms of mole fractions on Figure 6a for the present 5-species model, and on Figure 6b for a more complex model including 28 species taken from [10]. The comparison indicates a fairly good agreement particularly in the range of temperatures of interest here ($T \leq 15000\ K$).

The remaining tests were carried out for the inviscid reactive gas (Euler equations + dissociation model). The calculations were made over the 31×61 uniform mesh. The results for $M_\infty = 25$, 20 and 15 are shown on Figures 7,8 and 9 respectively. These include Mach/temperature contours, Mach/temperature plots and mass fraction plots. We observe that the gas dissociates essentially immediately after the shock. From the stagnation point, and along the body, as the flow accelerates, the temperature decreases, hence the dissociation is not as important, O_2 and N_2 eventually recombine. At $M_\infty = 25$, the maximum temperature observed at the stagnation point is approximately 25000 K, that is about 5000 K less than in the inert gas case. At $M_\infty = 15$, the predominant product is oxygen dioxyde, NO. However when the shock is stronger, $M_\infty = 25$ or even 20, the atomic species, O and N, dominate NO at least initially.

Finally, we note that a typical value for the CFL number is about 0.4 for the inviscid flow and about 0.2 for the viscous flow computations. To achieve steady-state convergence (a reduction of the residual L_2 norm of 10^{-4}) some 2000 explicit steps are usually sufficient. The convergence history of residual L_2 norm is indicated on Figure 10 in four cases, inviscid/viscous flow, with/without chemistry.

Generally speaking, we observe that the temperature levels have been diminished by the introduction of the dissociation phenomena. However these levels are still too high to be realistic. One immediate extension of our code will be realized by introducing an equilibrium model for the vibrational component in the energy. The importance of accounting for more species, or more complex phenomena such as ionization remains to be evaluated. Our current research is directed towards the development of a method for the solution of the non-equilibrium phenomena [8-9].

VI. CONCLUSION

A robust upwind finite-volume scheme has been developed to simulate the hypersonic reactive flow of equilibrium air governed by either the Euler or the Navier-Stokes equations.

The method includes a mesh-adaption procedure to sharply capture the strong shock. Some efforts are being made to render this procedure better adapted to Navier-Stokes calculations.

This code currently serves as a base of a more general program for the simulation of non-equilibrium hypersonic flow.

VII. ACKNOWLEDGMENTS

The authors would like to acknowledge the cooperation of B. Stoufflet and O. Le Ber, AMD-BA, St Cloud, who constructed the dissociation model.

Special thanks are also due to F. Fezoui and H. Stève, INRIA, Centre de Sophia Antipolis, who supplied the van Leer flux-splitting subprogram.

VIII. REFERENCES

[1] B. van LEER, "Flux-Vector Splitting for the Euler Equations", Lecture Notes in Physics, vol. 170, Aachen 1982, pp. 505-512.

[2] F. FEZOUI and H. STEVE, "Décomposition de flux de van Leer en éléments finis", to appear.

[3] A. DERVIEUX, J.A. DESIDERI, F.FEZOUI, B. PALMERIO, J.P. ROSENBLUM and B. STOUFFLET, "Euler calculations by upwind Finite Elements Methods and adaptative mesh algorithms", GAMM Workshop on the Numerical Simulation of Compressible Euler Flows, Rocquencourt (F), June 10-13 1986, to be published by Vieweg, Braunshweig-Wiesbaden.

[4] A. LERAT, "Propriété d'homogénéité et décomposition des flux en dynamique des gaz", Journal de Mécanique Théorique et Appliquée, Vol. 2, No. 2, 1983, pp. 185-213.

[5] B. STOUFFLET and M. O. LE BER, private communication.

[6] J. V. RAKICH, H. E. BAILEY and C. PARK, "Computation of Nonequilibrium Three-Dimensional Inviscid Flow Over Blunt-Nosed Bodies Flying at Supersonic Speeds", AIAA Paper 75-835, 1975.

[7] B. LARROUTUROU, "Adaptive numerical methods for unsteady flame propagation", Combustion and chemical reactors, G. S. S. Ludford Ed., Lectures in Appl. Math., 24 (2), 415-435, 1986.

[8] J. A. DESIDERI and N. GLINSKY, "Numerical Computation of the Chemical Dissociation and Relaxation Phenomena behind a Detached Strong Shock", INRIA Report to appear.

[9] J. A. DESIDERI, E. HETTENA and N. GLINSKY, "First Experiments with an Upwind Finite-Volume Solver for 2-D Non-Equilibrium Hypersonic Flow", INRIA Report to appear.

[10] W. G. VINCENTI and C. H. KRUGER, Jr., "Introduction to Physical Gas Dynamics", R. E. Krieger Publishing Company, J. Wiley & Sons, Inc., 1982, p. 174.

[11] J. D. ANDERSON Jr., "Modern Compressible Flow With Historical Perspective", McGraw-Hill Book Company, 1982.

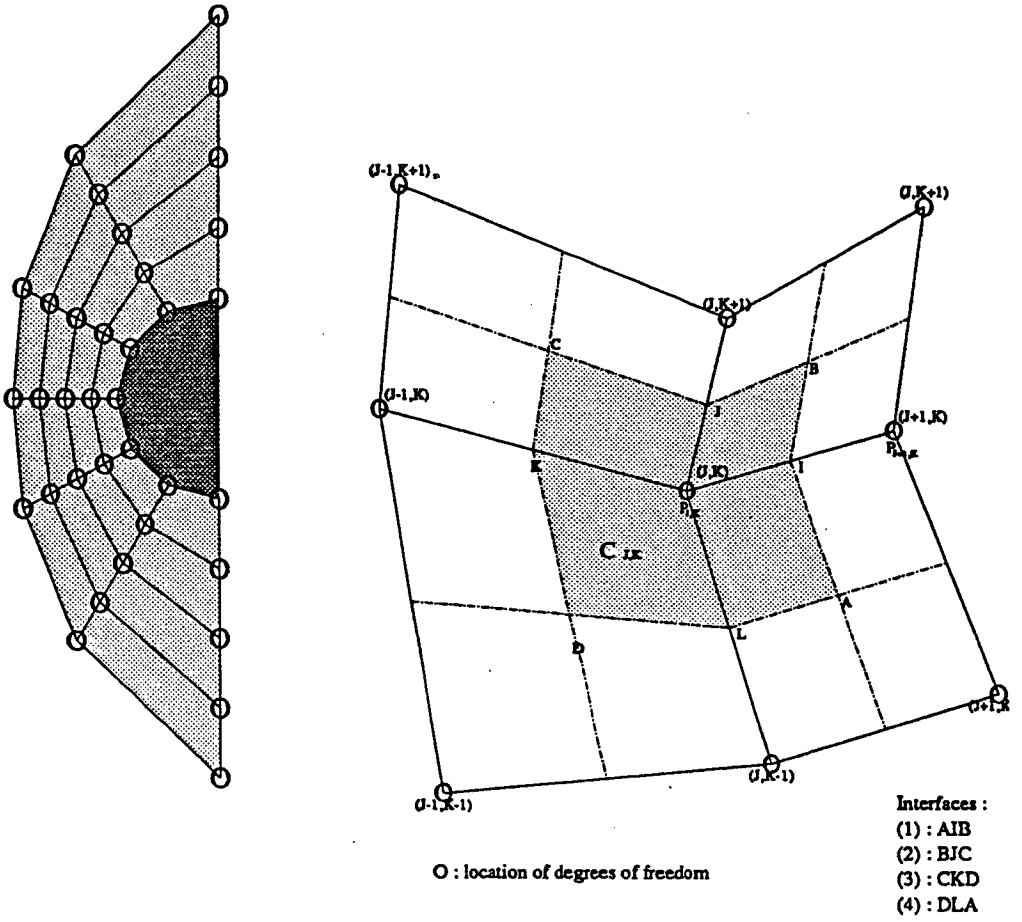

Figure 1 : Typical mesh and finite-volume cell

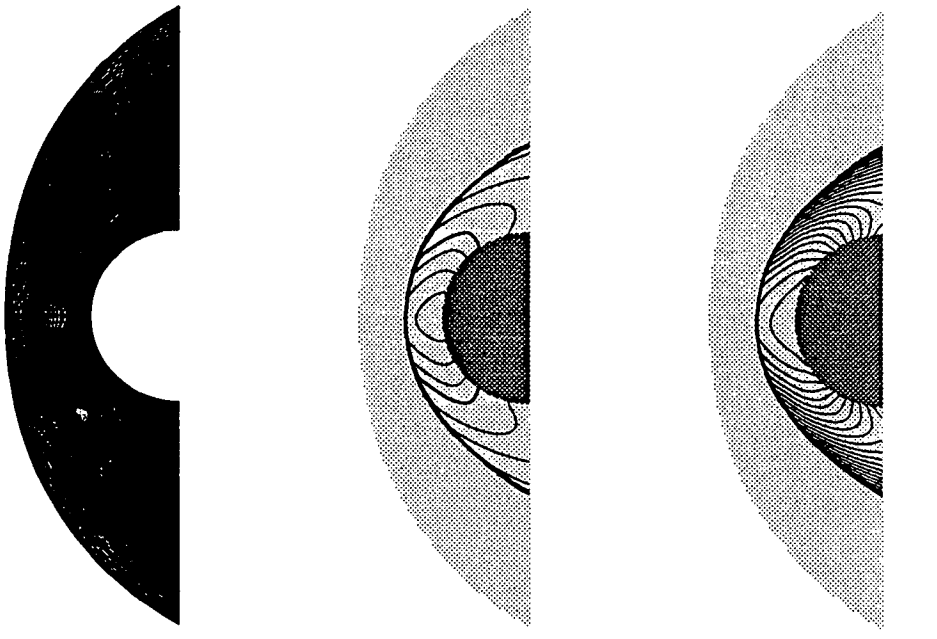

61x121 Mesh Mach lines Temperature lines

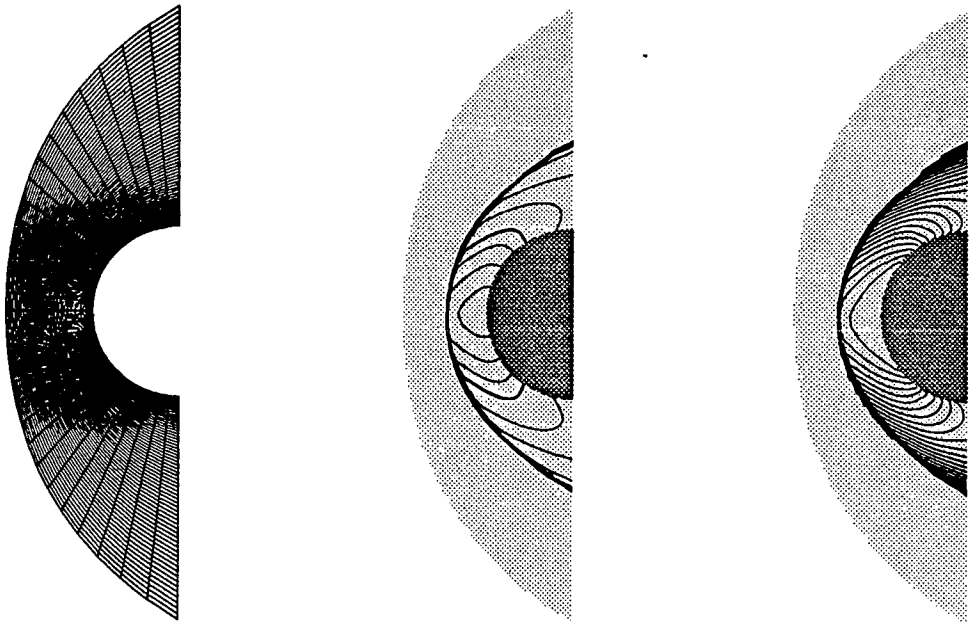

31x61 Mesh Mach lines Temperature lines

Figure 2 : Non reactive inviscid flowfield at $M_\infty = 25$
Validation test

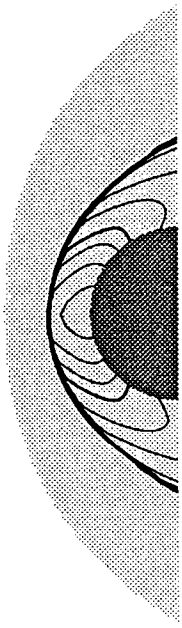

Mach lines ($M_\infty = 20$)

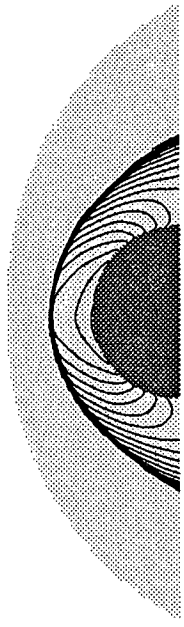

Temperature lines

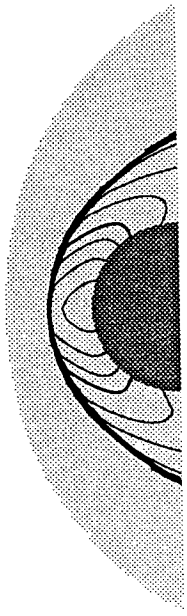

Mach lines ($M_\infty = 15$)

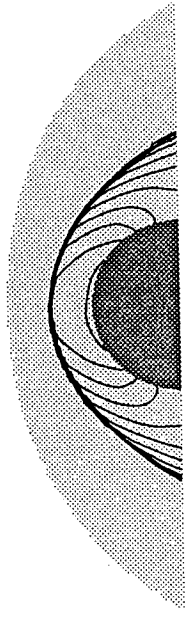

Temperature lines

Figure 3 : Effect of free stream Mach number on Mach and Temperature fields

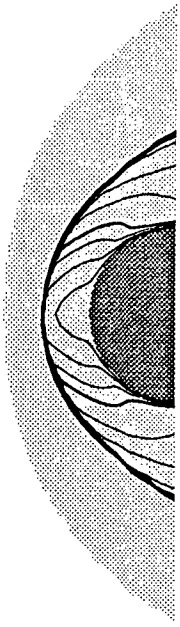

Mach lines ($M_\infty = 20$)

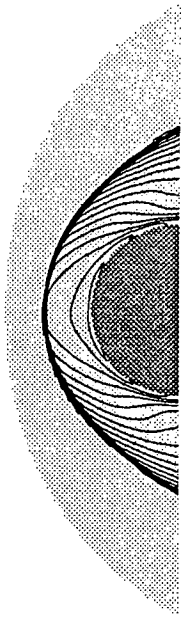

Temperature lines

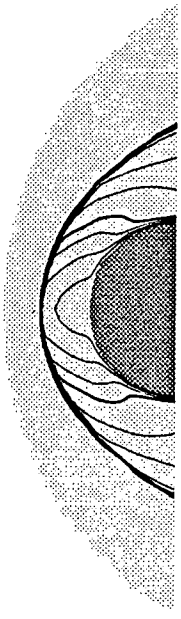

Mach lines ($M_\infty = 15$)

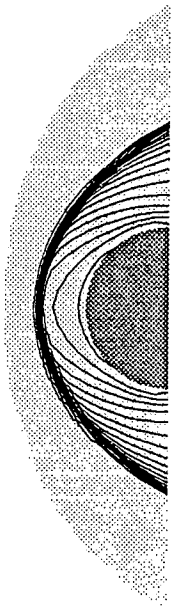

Temperature lines

Figure 4 : Effect of free stream Mach number on Mach and Temperature fields for navier-stockes at Re=1000

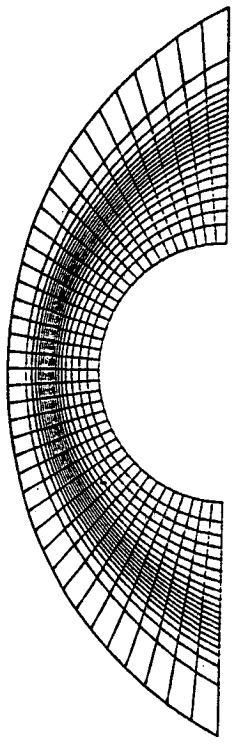

Grid

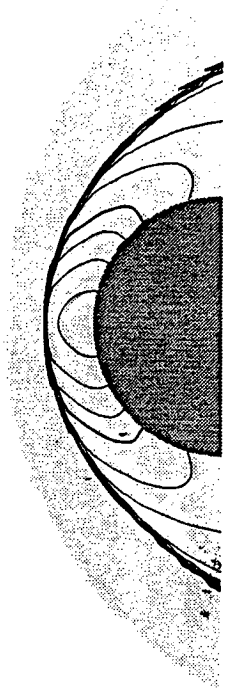

Mach lines

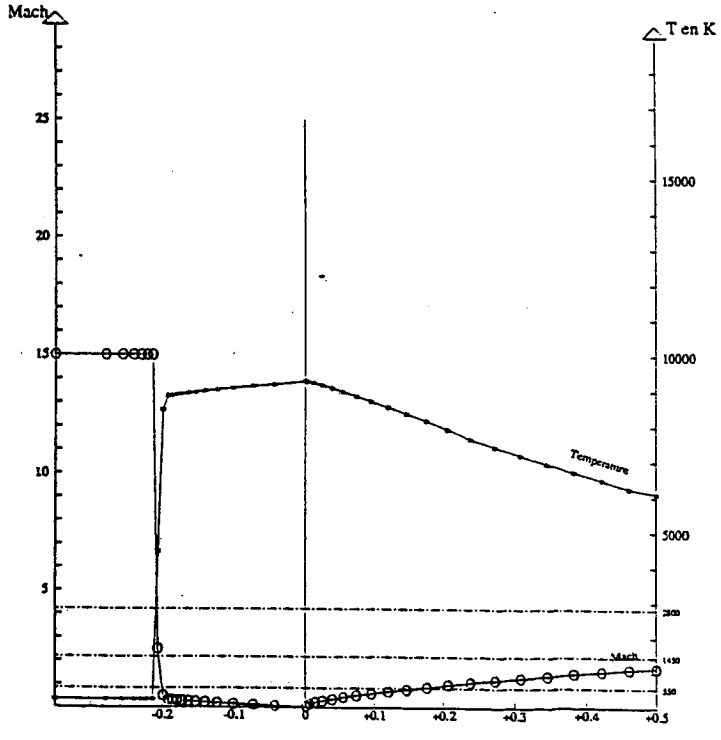

Figure 5 : Mesh adaption for an inviscid flow at $M_\infty = 15$ with a computational grid of 41 x 21 points

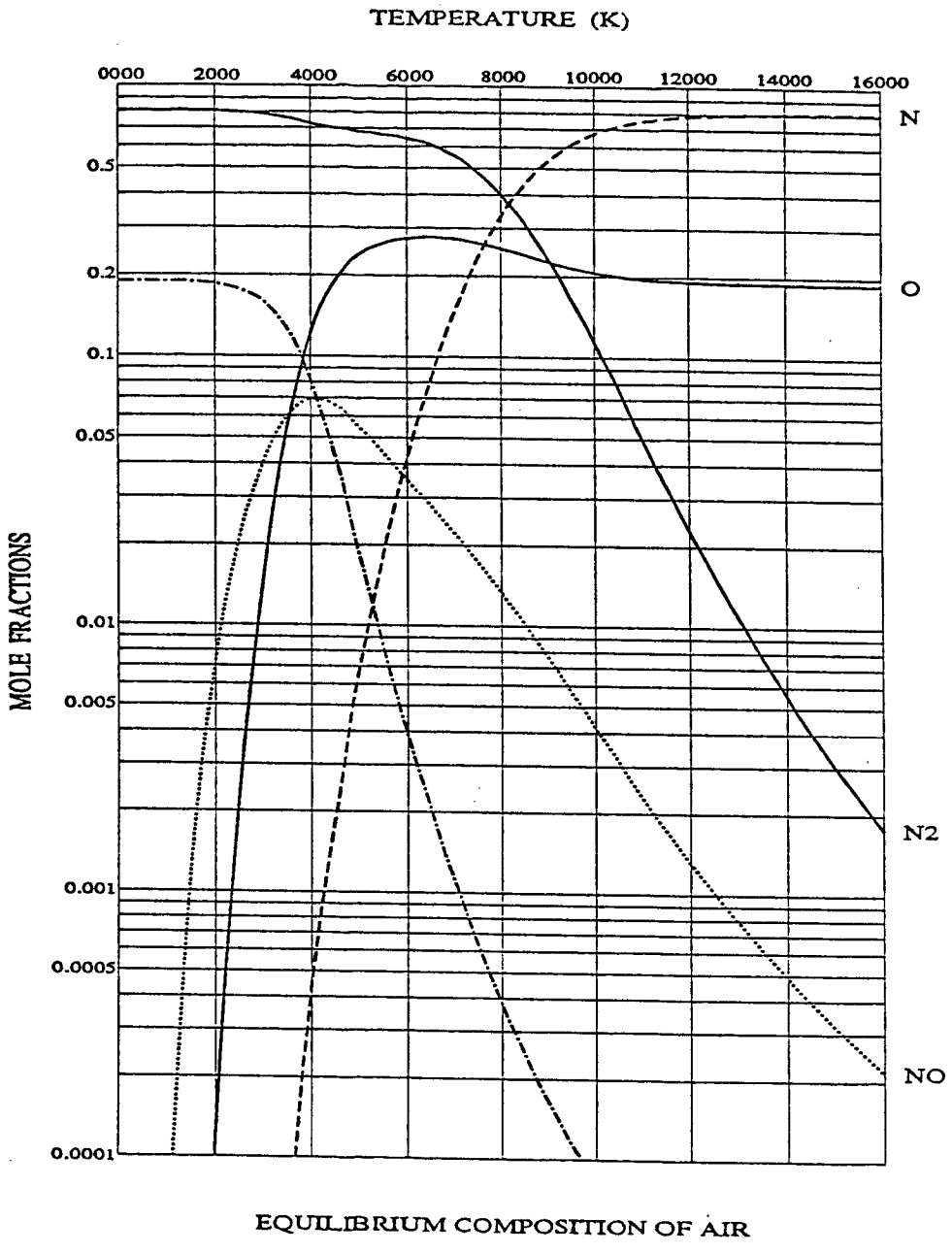

(a) Present 5-species model

Figure 6 : Comparison between equilibrium models ($p = 10^{-2}$ atm.)

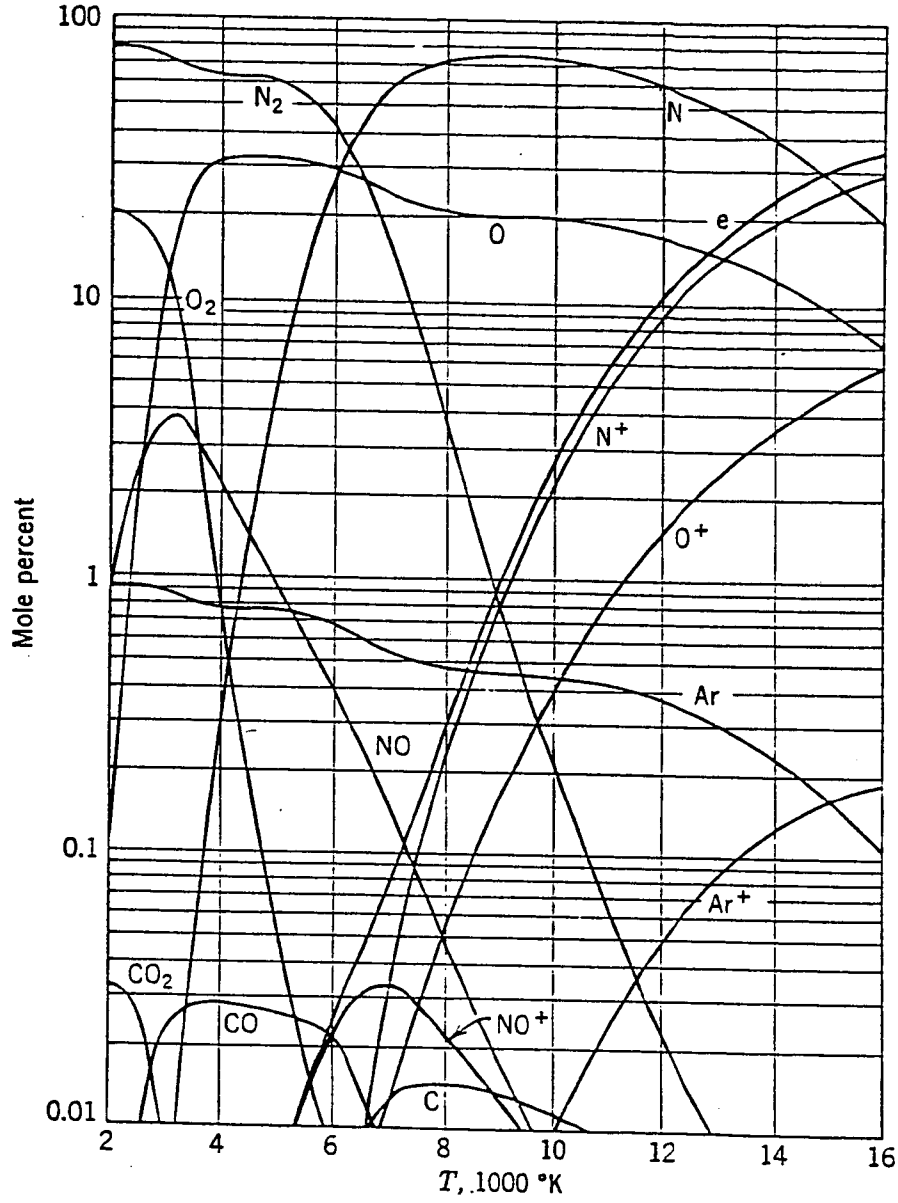

Fig. 4. Equilibrium composition of air at density of 10^{-2} atm (after Hilsenrath, Klein, and Woolley, 1959).

(b) 28-species model, from Vincenti-Kruger [10]

Figure 6 : end

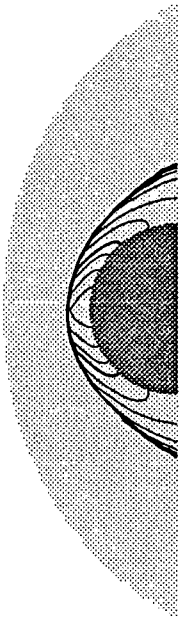

Mach lines ($M_\infty = 25$)

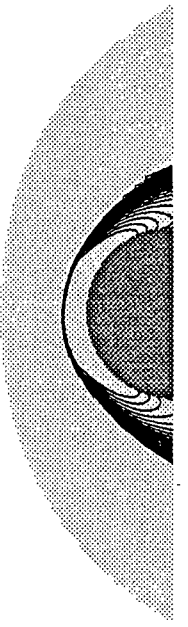

Temperature lines

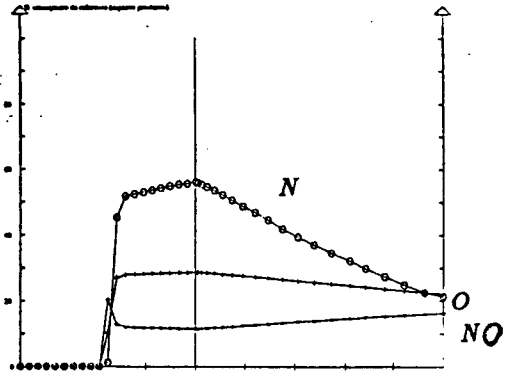

Mass fractions of N , O , NO

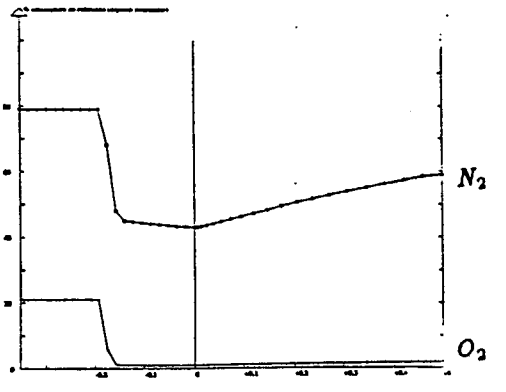

Mass fractions of N_2 , O_2

Figure 7 : Chemically reacting flow at $M_\infty = 25$

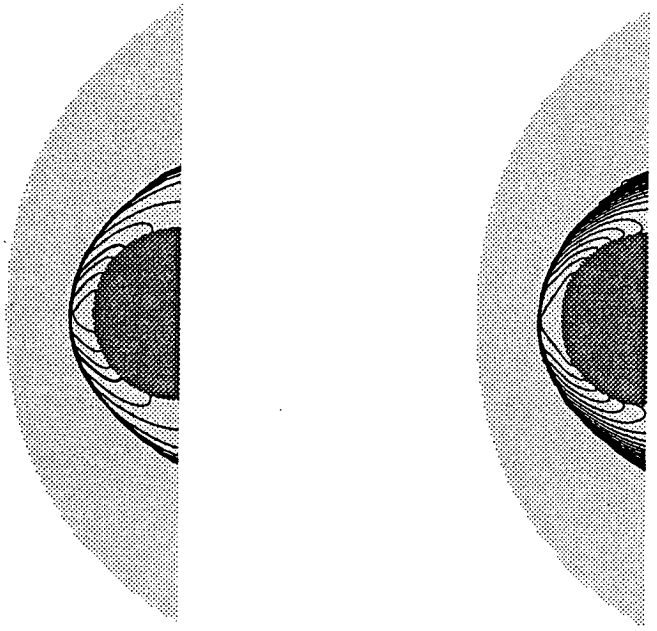

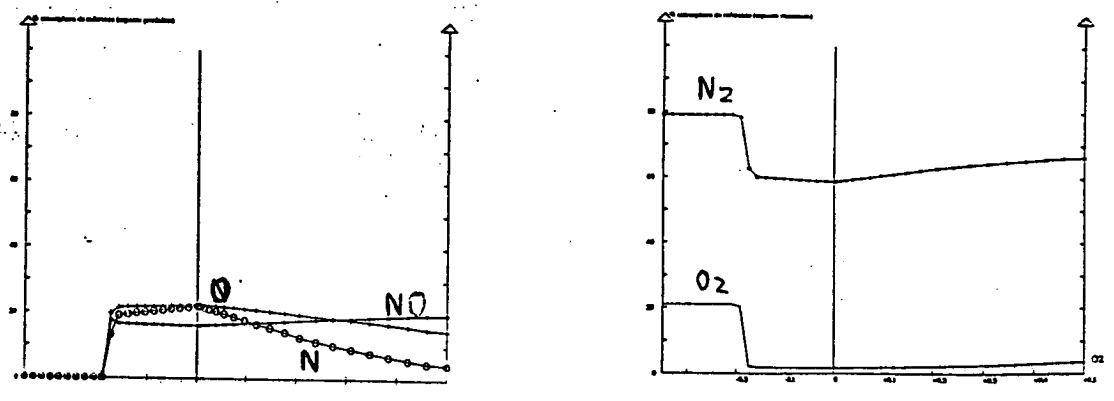

Figure 8 : Chemically reacting flow at $M_\infty = 20$

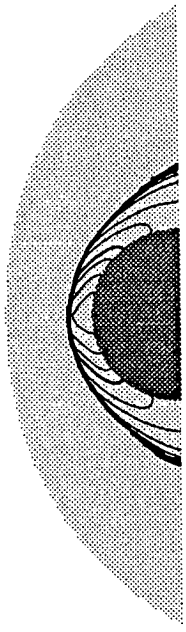

Mach lines ($M_\infty = 15$)

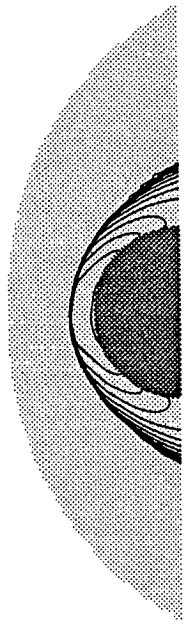

Temperature lines

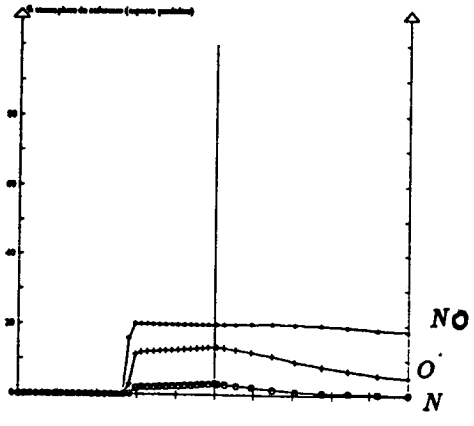

Mass fractions of N , O , NO

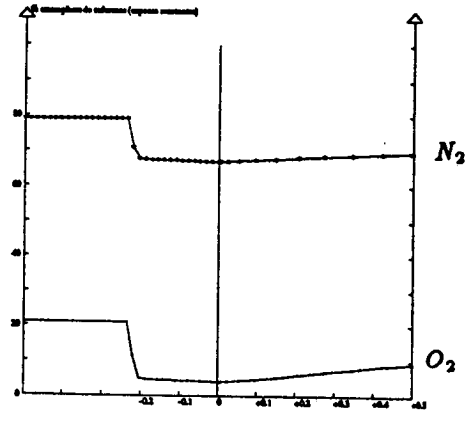

Mass fractions of N_2 , O_2

Figure 9.: Chemically reacting flow at $M_\infty = 15$

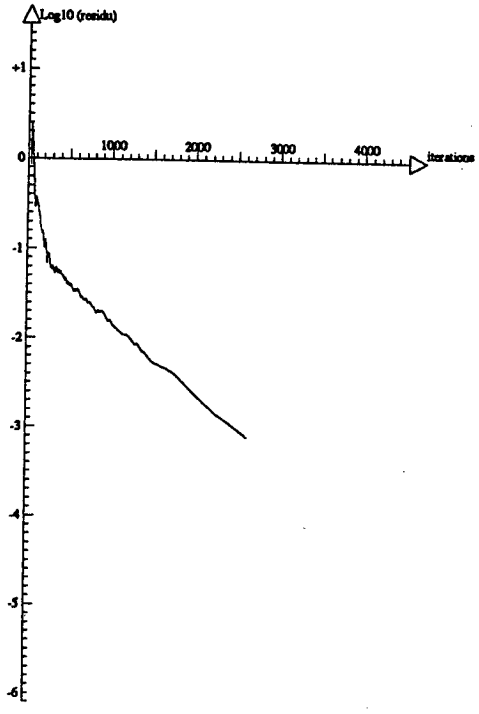

Euler flow

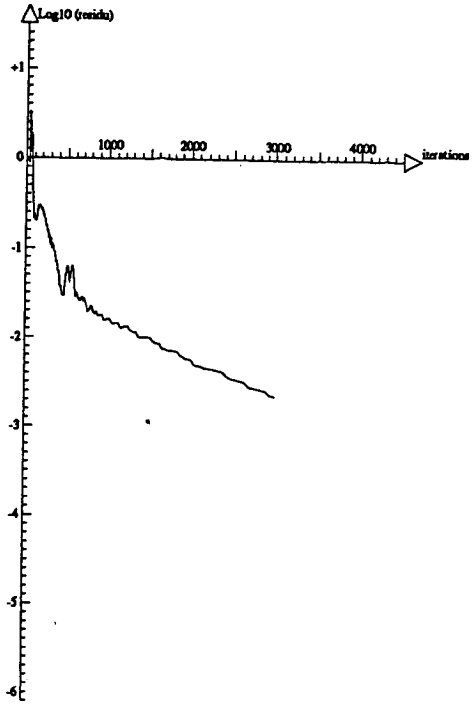

Navier-Stokes flow

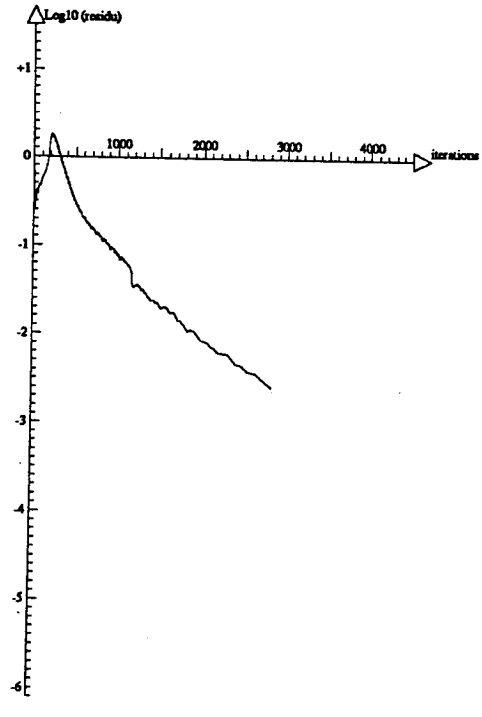

Chemically reacting flow

Figure 10 : Convergence history on a grid of 31 x 61 points ($M_\infty = 25$)